

Study of Morphologies of PMMA/PP/PS Ternary Blends

Ticiane S. Valera, Augusto T. Morita, and Nicole R. Demarquette*

University of São Paulo, Materials and Metallurgical Engineering Department, Av. Prof. Mello Moraes, 2463, 05508-900 São Paulo, Brazil

Received December 1, 2005

ABSTRACT: In this work, the morphologies of PMMA/PP/PS blends of different concentrations were studied and compared to the predictions of spreading coefficient, minimum free energy, and dynamic interfacial energy phenomenological models. Different morphologies than the ones predicted by the phenomenological models were observed in the case of PMMA matrix: a mixture of core–shell morphology (core of PP and shell of PS), dispersed PS, and subinclusions within the core when the concentration of PP was increased were obtained. The quantitative analysis of the morphologies indicated that when PMMA was the matrix, PS acted as an emulsifier. The study of the evolution of morphology in the case of 10/80/10 PMMA/PP/PS blends showed that when PMMA is added to the binary blend of PP/PS, threads of PMMA are formed and break up into droplets with a size comparable to the ones of PS forming a double dispersion type morphology, and then PMMA penetrates the drops of PS, forming a core–shell morphology with only one drop of PMMA inside a matrix. Subsequently, the core droplet of PMMA deforms and breaks up into smaller droplets.

1. Introduction

Polymer blends have been widely used in the industry because of their ability to combine in a unique material the properties of their components, at a relatively low cost when compared to the development of a new polymer.¹ Recently, the study and development of blends formed by three or more components has raised the attention of both the industrial and the academic world.^{2–16} It is well-known that the properties of polymer blends are greatly influenced by the morphology that is developed during the mixing process. In turn, the morphology is influenced by the following hierarchy of factors: interfacial tension > viscosity ratio > shear stress. Likewise, the morphology of ternary blends is also influenced by thermodynamics and kinetic factors.

Most of the papers on the subject of multiphase blends showed that the morphology of ternary blends can be predicted through the knowledge of interfacial tension between the components of the blends.^{2–4,7–16} In particular, Hobbs et al.⁷ used the concept of spreading coefficient and rewrote Harkin's equation in which two distinct phases are dispersed in a matrix phase to predict the morphology of ternary blends. In a ternary blend of three polymers **A**, **B**, and **C**, (supposing **A** is the matrix) the spreading coefficient, λ_{CB} , can be defined as

$$\lambda_{CB} = \alpha_{BA} - \alpha_{CA} - \alpha_{BC} \quad (1)$$

where λ_{ij} is the spreading coefficient of **i** over **j** and α_{ij} is the interfacial tension between **i** and **j**. For **B** to be encapsulated by **C**, λ_{CB} must be positive. In the case when both λ_{CB} and λ_{BC} are negative, **B** and **C** will tend to form separated phases. According to the signs of the spreading coefficient, for a given matrix, four types of morphologies can be obtained. They are summarized in Figure 1. In their original work, Hobbs et al.⁷ tested their model successfully for several ternary and quaternary blends including PMMA, PS, PC, PBT, and SAN, although the interfacial tension between the polymers involved was extrapo-

lated from room temperature. More recently, Guo et al.^{2,3} developed a new phenomenological model to predict the morphology of ternary blends, called here in this work the minimum free energy model. The authors derived an expression for the free energy of mixing of a multiphase blend, function of the interfacial area, and interfacial tension between each two components of the blend. The most stable morphology corresponds to the minimal free energy of mixing of the different morphologies shown in Figure 1. For any type of morphology, the free energy of mixing can be written as

$$G = \sum_i n_i \mu_i + \sum_{i \neq j} A_{ij} \alpha_{ij} \quad (2)$$

where μ_i is the chemical potential of **i**, n_i is the number of moles of **i**, A_{ij} is the interfacial area between components **i** and **j** and α_{ij} is the interfacial tension between components **i** and **j**. The first term of eq 2 is equal for all types of morphologies, but the second term differs from one morphology to another. Guo et al.^{2,3} evaluated the second term of equation for cases a–c of Figure 1 as

$$(\sum A_{ij} \sigma_{ij})_{B+C} = (4\pi)^{1/3} [n_B^{1/3} x^{2/3} \sigma_{AB} + n_C^{1/3} \sigma_{AC}] (3V_C)^{2/3} \quad (3a)$$

$$(\sum A_{ij} \sigma_{ij})_{B/C} = (4\pi)^{1/3} [n_B^{1/3} (1+x)^{2/3} \sigma_{AB} + n_C^{1/3} \sigma_{BC}] (3V_C)^{2/3} \quad (3b)$$

$$(\sum A_{ij} \sigma_{ij})_{C/B} = (4\pi)^{1/3} [n_B^{1/3} x^{2/3} \sigma_{BC} + n_C^{1/3} (1+x)^{2/3} \sigma_{AC}] (3V_C)^{2/3} \quad (3c)$$

where $x = V_B/V_C$, V_i is the volume fraction of phase **i**, n_B and n_C are the particles numbers of **B** and **C** phases. The lowest value of $\sum A_{ij} \alpha_{ij}$ will correspond to the lowest value of Gibbs energy of mixing, which can be considered as the most stable morphology.

Both the spreading coefficient and minimal free energy surface models have been used extensively to predict the morphology of ternary and quaternary blends,^{2–16} and it has

* Corresponding author. Telephone: 55 11 3091-5693. Fax: 55 11 3091-5243. E-mail: nick@usp.br.

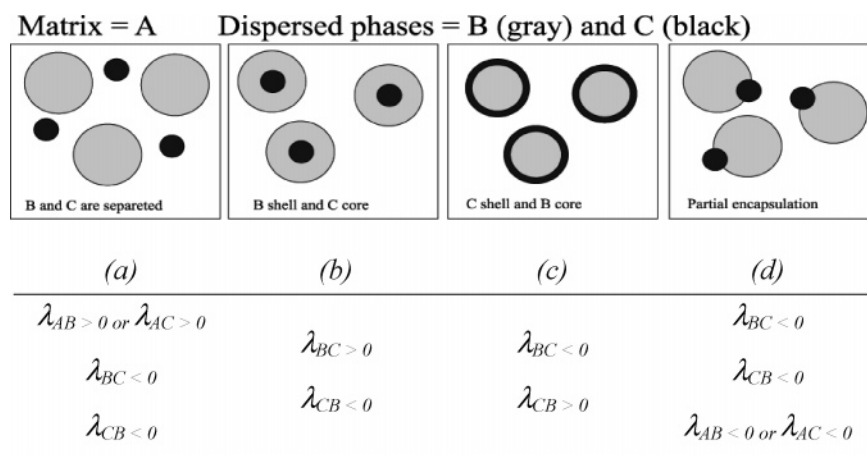


Figure 1. Some of the most common morphologies observed in ternary blends.⁴

Table 1. Characteristics of the Polymers Studied

polymer	supplier	grade	melt flow index
PS	Eni Chem	N1841	10 (200 °C/5kg)
PP	OPP	H306	15 (230 °C/2,16 kg)
PMMA	Metacril	01DHLE	4.2 (230 °C/3,9kg)

been shown that it is possible to control the morphology of those blends through compatibilization, which alters the respective values of interfacial tension.^{3,11,17,18} However, most of the studies conducted to predict the morphology of multiphase blends use interfacial tension data from the literature.⁸ Only few studies have used values of interfacial tension that were measured for the polymers studied.^{4–6,11} It is, however, well-known that the value of interfacial tension can be altered by the presence of small additives.¹⁹ Therefore, using values of interfacial tension from the literature instead of the ones measured for the polymers studied can lead to errors.

It has also been shown that the rheological properties of the polymers can affect the resultant morphology in ternary blends.^{12–17} In particular, the effects of viscosity^{12–16} and elasticity ratio¹⁷ of the two minor phases of a ternary blend on the resultant morphology have been studied. The conclusions regarding the effect of viscosity ratio are still, however, controversial. While some authors observed that the component of lower viscosity will encapsulate the component of higher viscosity,¹² some observed a contrary behavior,¹³ and some others did not see any influence of viscosity ratio on the type of morphology.^{5,16}

Reignier et al.,⁵ showed that in order to study the influence of viscosity ratio on the morphology of multiphase systems, the viscosity ratio should be estimated at a constant shear stress rather than at a constant shear rate, because the shear stress, rather than the shear rate, is continuous at the interface between the dispersed phase and the matrix phase. The authors⁵ also showed the influence of elasticity on the morphology obtained in ternary blends. Following Van Oene's work,²⁰ the authors developed a conceptual model to predict the encapsulation effects in composite droplet type systems based on a dynamic interfacial tension. Van Oene²⁰ demonstrated that, under conditions of dynamic flow, the elasticity differences between the components of a blend can alter the interfacial tension (called dynamic interfacial tension), and this tension can be quite different from the interfacial tension in the absence of flow. Reignier et al.⁵ introduced the dynamic interfacial tension term into the minimum free energy theory by Guo et al.,^{2,3} replacing

the static interfacial tension, obtaining the following equations:

$$(\sum A_i \sigma_{ij})_{B+C} = 4\pi R_i^2 \left[\sigma_{BA} + \frac{R_i}{6} (N_{1,B} - N_{1,A}) \right] + 4\pi R_i^2 \left[\sigma_{CA} + \frac{R_i}{6} (N_{1,C} - N_{1,A}) \right] \quad (4a)$$

$$(\sum A_i \sigma_{ij})_{B/C} = 4\pi R_e^2 \left[\sigma_{BA} + \frac{R_e}{6} (N_{1,B} - N_{1,A}) \right] + 4\pi R_i^2 \left[\sigma_{CB} + \frac{R_i}{6} (N_{1,C} - N_{1,B}) \right] \quad (4b)$$

$$(\sum A_i \sigma_{ij})_{C/B} = 4\pi R_e^2 \left[\sigma_{CA} + \frac{R_e}{6} (N_{1,C} - N_{1,A}) \right] + 4\pi R_i^2 \left[\sigma_{BC} + \frac{R_e}{6} (N_{1,B} - N_{1,C}) \right] \quad (4c)$$

where N_1 is the first normal stress difference for the phases **A**, **B**, and **C**, R_i and R_e are the internal and the external radius of the core–shell droplets, and σ_{ij} is the interfacial tension between the components *i* and *j*.

Using this new model, called here dynamic interfacial tension model, the authors were able to predict an unexpected encapsulation of PS by PMMA in a HDPE/PS/PMMA polymer blend (with a HDPE matrix) when constant shear stress is used replacing the constant shear rate. Moreover, they showed that the other predictive models described above were not able to predict such an effect.

In this work, the morphologies of PMMA/PP/PS blends with different compositions were investigated qualitatively and quantitatively. The qualitative results were compared to the spreading coefficient, minimum free energy theories, and the dynamic interfacial tension model. The interfacial tension for the different polymers pair involved was evaluated experimentally. The formation of morphology in the case of core–shell morphology was investigated. To our knowledge, the formation of morphology of a ternary blend has never been studied before.

2. Experimental Section

2.1. Materials. Commercial polypropylene (PP) from OPP S.A., poly(methyl metacrylate) (PMMA) from Metacril, and polystyrene (PS) from Enichem were used in this work. The properties of these polymers are listed in Table 1.

2.2. Blending and Sample Preparation. Binary and ternary blends were obtained by mixing the components of the blend in an internal mixer of a torque rheometer, at a temperature of 200 °C,

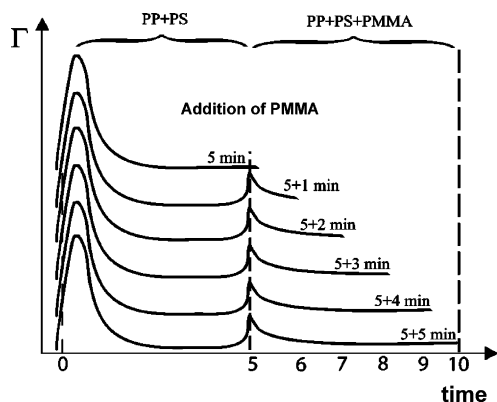


Figure 2. Schematic evolution of the torque (Γ) of the mixing chamber as a function of time for the samples used for the study of the evolution of morphology.

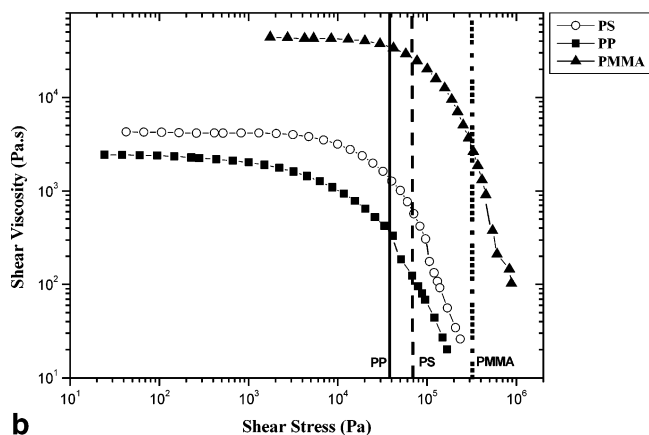
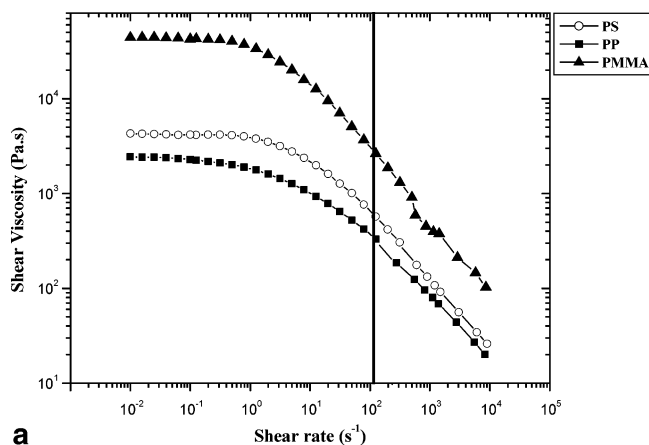


Figure 3. (a) Shear viscosity as a function of shear rate. (b) Shear viscosity as a function of shear stress, at a temperature of 200 °C, for the various polymers studied here.

Table 2. Viscosity of the Polymers at a Shear Stress That Corresponds to the Shear Stress Undergone by the Matrix Phase

shear stress of the matrix phase (Pa)	viscosity of the dispersed phase (Pa·s)		
	PP	PS	PMMA
PP, 39 490	370	1300	35 500
PS, 68 500	130	600	26 800
PMMA, 323 000	4	20	2700

with a rotor speed of 100 rpm, corresponding to a shear rate of roughly 115 s^{-1} .^{21,22} for 10 min. The binary blends were obtained to infer the interfacial tension between their components using rheological measurements following the analysis of Palierne²³ or Gramespacher and Meissner.²⁴ The binary blends were obtained in a 80/20 composition. The ternary blends were obtained in 80/05/

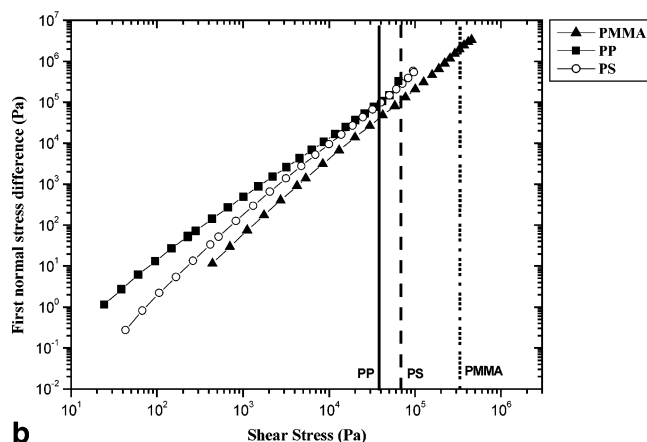
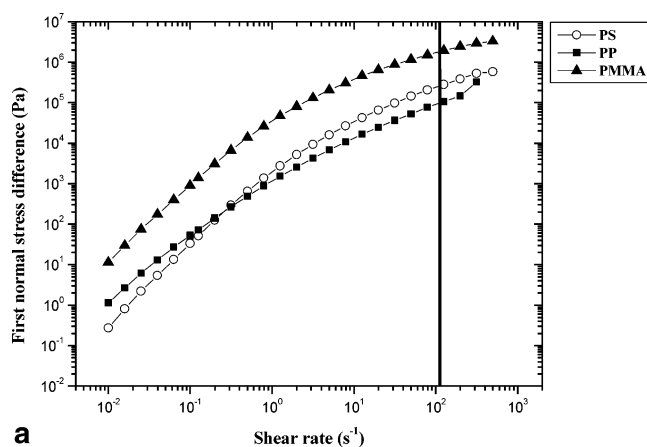


Figure 4. (a) First normal stress difference as a function of shear rate. (b) First normal stress difference as a function of shear stress, at a temperature of 200 °C, for each studied polymers.

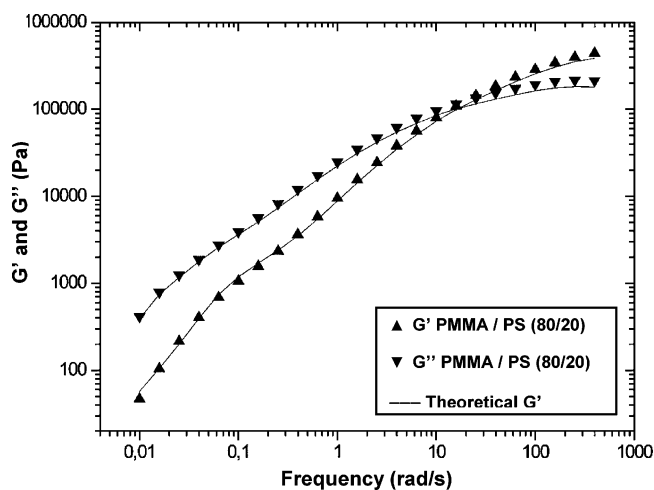


Figure 5. Comparison between the experimental storage modulus G' (ω) and loss modulus $G''(\omega)$ data and the best fit using the Palierne's model for 80–0–20 blend.

15, 80/10/10, and 80/15/05 composition. When PMMA was the matrix phase, the phenomenon of possible subinclusion formation of PS within the PP core was studied using the following compositions: 60/35/05, 60/30/10, 60/20/20, 60/10/30, and 60/05/35. These compositions were selected because of their improved morphology definition. The nomenclature used for the blends used in the following of the text is as follows: X–Y–Z corresponds to blends containing X vol % of PMMA, Y vol % of PP, and Z vol % of PS. All polymers were dried at 75 °C during 24 h prior to mixing. After processing, the blends were quenched in cold water to fix the morphology. After quenching, samples of ternary blends, binary

Table 3. Parameters Used for the Calculation of Interfacial Tension from Rheological Data^a

	PMMA/PP	PMMA/PS
R_v (μm)	5.5	0.28
R_n/R_v	3.7	1.4
Φ (%)	20	20
η_{om} (Pa·s)	1.03×10^5	1.03×10^5
η_{od} (Pa·s)	8.13×10^3	1.25×10^4
K	0.08	0.12

^a R_n is the number-average radius of the dispersed phase, R_v is the volume average radius, Φ is the volume fraction of the dispersed phase, η_{om} is the zero shear viscosity of the matrix, η_{od} is the zero shear of the dispersed phase, and K is the viscosity ratio.

Table 4. Interfacial Tensions between the Polymers of PMMA/PP/PS Ternary Blends

polymers	experimental value (mN m ⁻¹)	literature (mN m ⁻¹)	harmonic mean (mN m ⁻¹) ^{33–34}
PP/PS	5.68	6.25 ²⁷	5.0
PMMA/PP	7.50	—	7.7
PMMA/PS	1.69	1.5 ⁴	1.01

Table 5. Predicted Equilibrium Morphology for PMMA/PP/PS Ternary Blends^a

(a) Morphology Predicted by Spreading Coefficient									
polymer pairs				λ (mN/m) \pm 0.7					
PMMA/PS				−3.51					
PS/PMMA				0.13					
PP/PS				−11.49					
(b) Morphology Predicted by Minimal Surface Energy									
vol fraction (Φ_B/Φ_C)	PMMA (matrix) PP = B, PS = C			PP (matrix) PMMA = B, PS = C			PS (matrix) PP = B, PMMA = C		
	B + C	B/C	C/B	B + C	B/C	C/B	B + C	B/C	C/B
1	42.5	81.4	41.0	61.5	52.1	62.5	36.0	47.5	77.6
0.33	32.6	90.0	30.8	61.8	54.8	59.3	41.4	58.1	65.0

^a Φ_i is the volume fraction of polymer i .

blends, and single polymers (which had undergone the same thermomechanical treatment) were prepared for morphological observations and rheological measurements, respectively. Disks of 25 mm diameter and 1.5 mm thickness were molded at 200 °C, under a pressure of 18 MPa, during 15 min. This 15 min corresponded to the time at which the morphology of the binary blends was of a dispersion of droplets dispersed in a matrix; this type of morphology is necessary if one wants to evaluate the interfacial tension between two polymers using the rheological behavior of the blend formed by those two polymers.^{23,24}

To study the formation of the morphology of a ternary blend in an internal mixer, several samples of the ternary blend 10–80–10 were prepared as a function of processing time and their morphology was studied by scanning electron microscopy. A blend with a PP matrix was chosen to enable the dissolution of both dispersed phases. Preliminary experiments performed at a rotor speed of 100 rpm showed that the final morphology was obtained within the first 2 min of mixing, corroborating the results of Reignier et al. for

HDPE/PS/PMMA blends.⁴ These rotor speeds were too high to enable the study of the formation of morphology. Therefore, a rotor speed of 30 rpm was used in the study of the evolution of the morphology of the ternary blend. In a first step, PP and PS were mixed together for 5 min (necessary time to obtain a droplet dispersion type morphology) and then, PMMA was added to the blend. Samples of the ternary blends were then removed from the mixer chamber as a function of time. Figure 2 shows schematically the torque in the mixing chamber as a function of time for the different samples studied.

2.3. Interfacial Tension. Several methods can be used to infer interfacial tension between molten polymers.²⁵ More details can be found in a recent review paper written by Demarquette.²⁶ In this work, the pendant drop method, breaking thread method, and the possibility of inferring interfacial tension from the rheological behavior of the blend were tested for the different polymer pairs, PS/PP, PMMA/PP, and PMMA/PS. It was not possible to infer the interfacial tension for polymer pairs involving PMMA using the pendant drop and breaking thread method due to the high viscosity of PMMA and lack of index of refraction difference in the case of PMMA and PS. Therefore, the interfacial tension for the pairs of polymers involving PMMA were determined using the rheological behavior of their respective blend. The data were analyzed using Palierne and Gramespacher and Meissner's^{23,24} analyses following the procedures reported elsewhere.^{27–29} Due to the higher accuracy of the method the pendant drop method was used for PP/PS polymer pair. The apparatus used in this work and the experimental procedures have been described in several works of this research group.^{30,31}

2.4. Rheological Characterization. The shear viscosity of the polymers as a function of shear rate was evaluated using a capillary rheometer Instron 4467 at a temperature of 200 °C. The die used had a diameter of 0.04 mm and L/D of 50. A Rabinowitch correction was applied to the experimental results. All the samples were dried under vacuum at a temperature of 70 °C for 4 h prior to the rheological measurements.

The rheological tests, necessary for the evaluation of interfacial tension, were carried out using a Rheometric Scientific SR-5000 rheometer under dry nitrogen atmosphere. A parallel-plate configuration was used with a gap size of 1 mm and a plate diameter of 25 mm at a temperature 200 °C, under a nitrogen atmosphere. Strain and stress sweep tests were performed for all blends and pure polymers to define the linear viscoelasticity region. Dynamic frequency sweeps were performed for the binary blends and pure components. The zero shear viscosities of the polymers necessary to infer the interfacial tension from rheological measurements were inferred using Carreau's equation.³²

2.5. Morphology. The morphology of all the blends was characterized by scanning electron microscopy. The blend samples were fractured cryogenically and then covered with gold in a Balzers sputter coater (model SCD-050). To obtain a good contrast between the phases in ternary blends, dissolution of one of the phase was carried out whenever possible. The PMMA and PS were dissolved with acetic acid and cyclohexane, respectively. Quantitative analysis of the morphology was performed using Carl Zeiss Vision KS-300 software. In the case of the quantitative analysis of the

Table 6. Values of the Dynamic Interfacial Energy for PMMA/PP/PS Ternary Blends^a

dynamic interfacial energy (N m/particle)									
	PMMA (matrix) PP = B, PS = C			PP (matrix) PMMA = B, PS = C			PS (matrix) PP = B, PMMA = C		
	B + C	B/C	C/B	B + C	B/C	C/B	B + C	B/C	C/B
shear	5.4×10^{-12}			1.6×10^{-13}			1.9×10^{-13}		
stress		3.8×10^{-12}	5.9×10^{-12}		2.6×10^{-13}	1.4×10^{-13}		4.1×10^{-13}	2.1×10^{-13}
constant	3.7×10^{-12}			1.6×10^{-13}			1.0×10^{-13}		
shear	1.9×10^{-12}			4.2×10^{-12}			3.7×10^{-12}		
rate		5.7×10^{-13}	1.2×10^{-13}		7.5×10^{-12}	4.1×10^{-12}		6.7×10^{-12}	4.1×10^{-12}
constant	1.1×10^{-13}			4.2×10^{-12}			3.4×10^{-12}		

^a The asterisk denotes results obtained using the assumption made by Reignier et al.,⁵ i.e.: $R_c = R_i$.

Table 7. Qualitative Results of the Morphology of the Ternary Blends

Matrix	Blend Composition	Morphology predicted by spreading coefficient	Morphology predicted by minimal surface energy	Morphology predicted by dynamic interfacial tension model	Morphology observed experimentally
PMMA	80-05-15	Core-shell morphology with a core of PP and shell of PS	Core-shell morphology with a core of PP and shell of PS	Shear stress constant: Core-shell morphology with a core of PS and shell of PP	Mixture of Core-shell morphology with core of PP and shell of PS and droplets of PS
PMMA	80-10-10			Shear rate constant: Core-shell morphology with a core of PP and shell of PS	(subinclusions of PS in the core of PP to PP content >75vol%)
PMMA	80-15-05				
PP	05-80-15	Core-shell morphology with a core of PMMA and shell of PS	Core-shell morphology with a core of PS and shell of PMMA	Shear stress constant: core-shell morphology with a core of PMMA and shell of PS	Core-shell morphology with a core of PMMA and shell of PS
PP	10-80-10			Shear rate constant: core-shell morphology with a core of PMMA and shell of PS	
PS	10-10-80	Separated dispersion of PMMA and PP	Separated dispersion of PMMA and PP	Shear stress constant: Separated dispersion of PMMA and PP	Separated dispersion of PMMA and PP
PS	15-05-80			Shear rate constant: Separated dispersion of PMMA and PP	

Table 8. Quantitative Results of the Morphology of the Ternary Blends (d_v)

blend composition	vol av diameter, d_v (μm)		
	PMMA	PP	PS
80/05/15 (core shell) dispersed PS		0.63	0.83
80/10/10 (core shell) dispersed PS		0.99	1.22
80/15/05 (core shell) dispersed PS		1.71	1.88
			0.10
05/80/15	0.93		22
15/5/80	0.78	1.4	
10/10/80	0.44	2.63	

morphology of the binary blend, necessary to evaluate interfacial tension using rheological measurement, about 10 000 particles were measured for all cases, and Saltikov's correction³³ was used.

3. Results and Discussion

3.1. Rheological Characterization. Figure 3a shows the viscosity of the different polymers as a function of shear rate or frequency, and Figure 3b shows the viscosity of the polymers as a function of shear stress. The vertical line in Figure 3a represents the applied shear rate, and the vertical lines in Figure 3b represent the matrix phase shear stress undergone by the matrix for each matrix phase.

It can be observed in Figure 3a that for the velocity of processing studied, corresponding to an average shear rate of 115 s^{-1} , the range of viscosity is $\eta_{\text{PMMA}} > \eta_{\text{PS}} > \eta_{\text{PP}}$. Table 2 presents a summary of the results in Figure 3b, showing the viscosity for all the polymers at a shear stress that corresponds to the shear stress undergone by the matrix phase. The values of the viscosity of PP and PS at the shear stress undergone by PMMA matrix phase were obtained by extrapolation of the data. From Table 2 and Figure 3b, it can be seen that the range of viscosity is $\eta_{\text{PMMA}} > \eta_{\text{PS}} > \eta_{\text{PP}}$.

The first normal shear stress difference for the studied polymers was calculated using the empirical correlation developed by Laun.³⁴ Parts a and b of Figure 4 present the first normal stress difference for each studied polymer as a function of shear rate and shear stress, respectively. It can be observed for an average shear rate of 115 s^{-1} , which corresponds to the one to which the blends were submitted to in the mixer, the normal shear stress differences range in the following order $N_{1\text{PP}} < N_{1\text{PS}} < N_{1\text{PMMA}}$. However, for the range of shear stresses studied (see Figure 4b), the normal shear stress difference of PMMA is lower than the one of PP or PS which are of the same order of magnitude within experimental error.

3.2. Interfacial Tension, Spreading Coefficient, Minimum Free Energy and Dynamic Interfacial Tension Models. The interfacial tension between PP and PS at a temperature of 200°C was evaluated using the pendant drop method and was found equal to $5.68 \pm 0.09 \text{ mN m}^{-1}$ corroborating results obtained in other works.^{25,29,35} Figure 5 shows a comparison between the experimental data of storage modulus $G'(\omega)$ and loss modulus $G''(\omega)$ for 80-0-20 blend and the best fit using Palierne's model. It can be seen that a good fit is obtained between experiments and theory for the whole range of frequencies. It can also be seen, that a secondary plateau of $G'(\omega)$ is observed for frequency ranging from 0.2 to 0.5 rad/s. This secondary plateau corresponds to the relaxation of the dispersed phase when sheared. Similar result was obtained for 80-20-0 binary blend. The fit of Palierne's model to the experimental data was used together with the data reported in Table 3 to calculate the interfacial tension for those three blends. Although, the rheo-

logical method is certainly the least precise method to evaluate interfacial tension between polymers,^{26,38} the reproducibility of the data found here was within 10%.

Table 4 shows the values of interfacial tension obtained for the different polymers pairs used in this work at a temperature of 200 °C. These values were used to predict the morphologies of the ternary blends. In Table 4, the values of literature as well as the ones obtained by harmonic means for the same polymer pairs are also shown, and it can be seen that the results obtained corroborate the ones from literature and the ones obtained by harmonic means.^{36,37}

Table 5a shows the values of the spreading coefficient (calculated using the interfacial tension values measured in this work), and Table 5b shows the second term of the right-hand side of eq 2, for the studied blends. Table 6 shows the values of the dynamic interfacial energy of all blends, obtained from eq 4, parts a–c, using the first normal stress difference values obtained at constant shear rate and shear stress (see Figure 4, parts a and b). To calculate the dynamic interfacial energy, it was assumed, following Reignier et al.'s⁵ work that all the studied structures have the same number of particles of the dispersed phase, $R_i = 1 \mu\text{m}$, negative values of the dynamic interfacial tension could be set equal to zero and that for core-shell morphologies (B/C or C/B) $R_e = \sqrt[3]{2}R_i$. To calculate the dynamic interfacial energy in the case of separated dispersion of both dispersed phases (B + C) differently from the work of Reignier et al.,⁵ who assumed that in this case $R_e = R_i$, two cases were considered.

(i) when $\gamma_{AB} \approx \gamma_{BC}$ (where γ_{AB} is the interfacial tension between polymers A and B and γ_{BC} is the interfacial tension between polymers B and C), which is the case when PP is the matrix $R_i = R_e$.

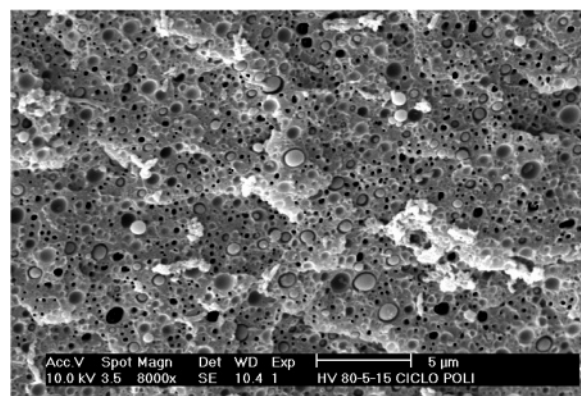
(ii) when γ_{AB} differs from γ_{BC} , which is the case when either PMMA or PS are the matrix, the ratio between R_i and R_e was obtained from the experimental values of R_i and R_e found in the binary blends, assuming volume conservation. When PMMA was the matrix these assumptions resulted in $R_i = R_e/20$. When PS was the matrix the values of R_i and R_e were obtained directly from the PMMA and PP droplets in the ternary blend (Table 8, 10/10–80 blend).

These assumption resulted in a possible minimum of dynamic interfacial energy (D.I.E) for morphologies different from the B + C morphology as can be seen in Table 6; when considering $R_e = R_i$, the dynamic interfacial energy will always show a minimum value for B + C morphology as pointed out by Reignier et al.⁵

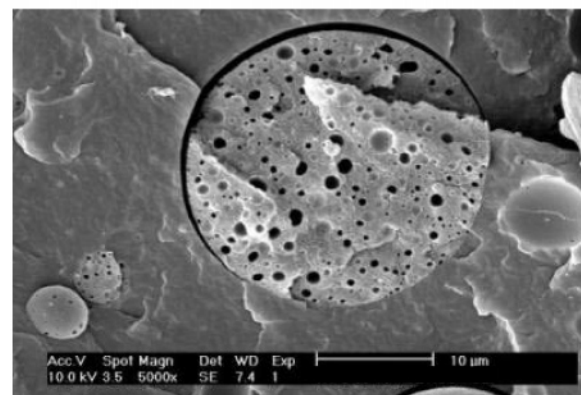
In the calculation of the D.I.E., the uncertainty on the value of interfacial tension was also taken into consideration. The D.I.E. was calculated using the values of interfacial tension reported in Table 4 and using the values of interfacial tension $\pm 30\%$, which corresponds to the experimental error on the interfacial tension.^{26,38} The D.I.E., which is reported in Table 6, corresponds to the average of the three values obtained. For the prediction of the D.I.E., the results following the assumption made by Reignier et al.⁵ (i.e., $R_e = R_i$) and the ones following the assumption made in this work (see above) are reported. It can be seen that when the assumption $R_e = R_i$ is made the D.I.E. always shows a minimum value for B + C morphology.

The results of the predicted morphologies are shown in Table 7. The following can be seen, for all blends, according to the minimal surface free energy model:

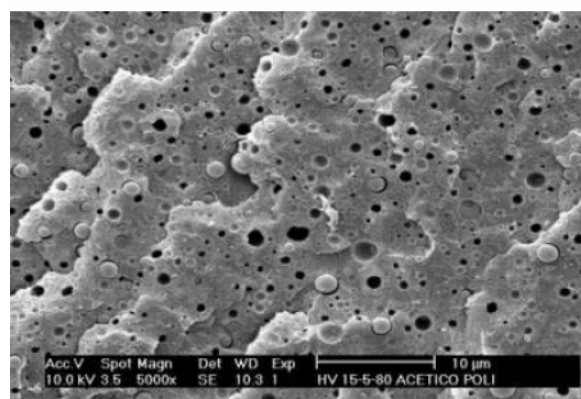
(i) When PMMA is the matrix, a core-shell morphology with PP as core and PS as shell should be obtained.



a



b



c

Figure 6. Morphology of PMMA/PP/PS ternary blend: (a) (80/5/15) after cyclohexane etching; (b) (5/80/15) after acetic acid etching; (c) (15/5/80) after acetic acid etching.

(ii) When PP is the matrix, a core-shell morphology with PS as core and PMMA as shell should be obtained.

(iii) When PS is the matrix, a separated dispersion morphology of PMMA and PP should be obtained.

It can be also seen in Table 7 that, for all studied blends, the predictions of the spreading coefficient model corroborated with the morphology predicted by the minimal surface free energy except in the case of PP. Using the dynamic interfacial tension model, the following morphologies can be predicted.

(i) When PMMA is the matrix, a core-shell morphology, should be obtained. When values of N_1 at constant shear stress are considered in the calculations, the core and shell should be formed by PS and PP respectively, whereas the core and shell should be formed by PP and PS respectively when values of N_1 at constant shear rates are considered.

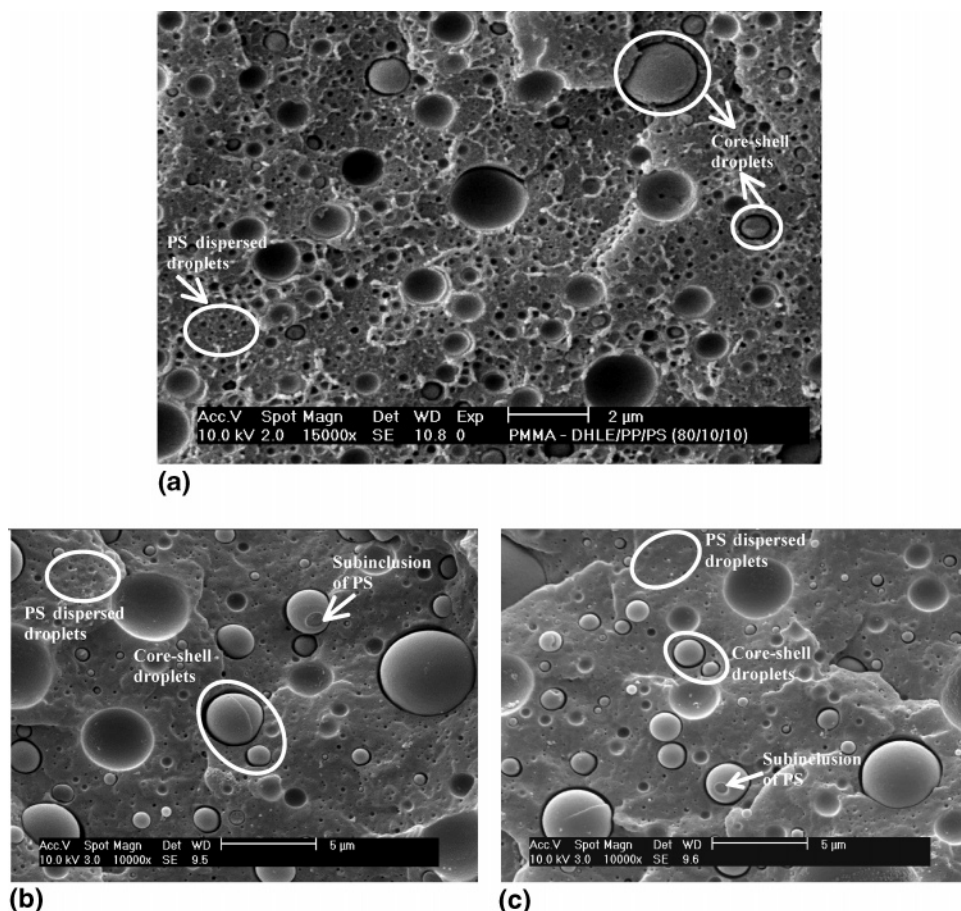


Figure 7. Morphology of PMMA/PP/PS ternary blend: (a) (80/10/10) after chemical attack with cyclohexane; (b and c) (80/15/05) after chemical attack with cyclohexane.

(ii) When PP is the matrix, a core-shell morphology with PMMA as core and PS as shell should be obtained when values of N_1 at either constant shear stress or shear rate are considered.

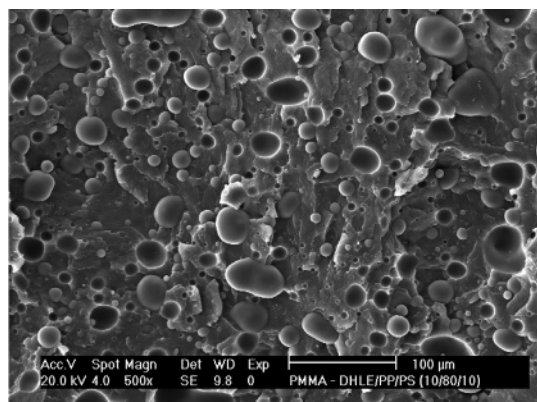
(iii) When PS is the matrix, a separated dispersion of PS and PMMA should be obtained.

3.3. Blend Morphology. Parts a–c of Figure 6 show a typical type of morphology for each matrix studied. The pictures correspond to a concentration of the dispersed phase of 5/15. When the matrix phase was formed by PMMA (Figure 6a), the PS was dissolved using cyclohexane, when the matrix phase was formed by PP (Figure 6b) or PS (Figure 6c) the PMMA was dissolved using acetic acid. In the case of ternary blends with PMMA as matrix phase, a mixture of morphologies was observed: core-shell morphology with PS as shell and PP as core and droplets of PS dispersed in the matrix phase. In the case of the ternary blend with PP as a matrix phase, it can be seen that the phase inside the droplets was dissolved, showing that, in this case a core-shell morphology was also obtained. In this case, the PS encapsulated the PMMA. In the case of the ternary blend with PS as a matrix phase, it can be seen that the acetic acid dissolved the PMMA phase, leaving small holes within the PS matrix phase, while the PP phase remained dispersed within the PS matrix showing that the possible morphology when PS is the matrix phase is a dispersion of separated drops of PMMA and PP. Similar qualitative results were obtained for concentrations of the dispersed phase of 10/10 when PS was the matrix phase. When PMMA was the matrix phase, increasing the PP content from 10 to 15 resulted in a new mixture of morphologies: core-shell morphology with PS as shell and PP as core, subinclusions of PS shell in the core of PP droplets, and PS dispersed droplets (see Figure 7a for the

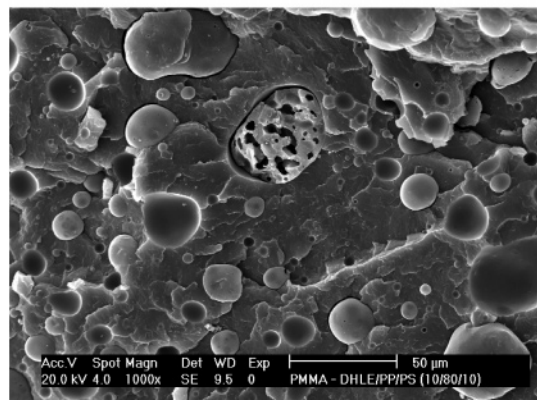
80/10/10 blend and Figure 7, parts b and c, for the 80/15/05 blend). Similar types of microinclusions have been observed by Favis et al.⁶ In the case of a concentration of the dispersed phase of 10/10 and a matrix of PP a cocontinuous phase morphology was obtained in the core-shell dispersed phase as can be seen in Figure 8. Table 7 summarizes and compares the qualitative experimental results obtained to the predictions of the different phenomenological models studied here.

The predicted morphologies by spreading coefficient model corroborate the morphologies experimentally observed for ternary blends in most of the cases. The predicted morphology by minimal free energy only corroborates the experimental ones in the case of a matrix of PS: in the case of a matrix of PP, the model is not able to predict the encapsulation of the PMMA by PS. When PMMA is the matrix, neither the spreading coefficient model nor the minimal free energy model predicts the mixture of morphologies obtained experimentally, the core-shell morphology (core of PP and shell of PS) and droplets of dispersed PS, since the models predict only the presence of a core-shell structure. In the case of the minimal surface energy theory, a closer look at the values of surface energy presented in Table 5 reveals that, for PMMA matrix, the differences between the values of the surface energy for the dispersed phase morphology and the ones for the core-shell morphology are small, lying within experimental error.

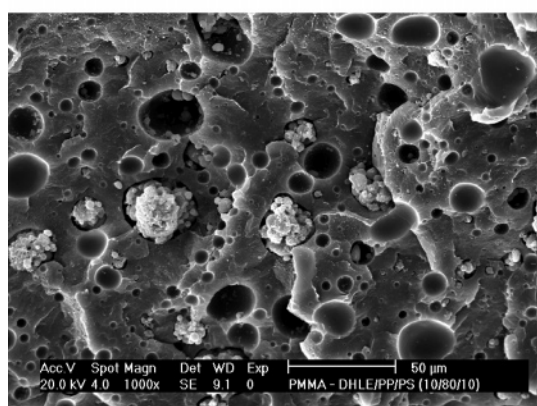
It can be also seen from Table 7 that the D.I.E. model predictions corroborate the experimental results for PS and PP matrix and PMMA when values of N_1 at constant shear rates were considered in the model prediction, when R_i was assumed to be different from R_e .



a



b



c

Figure 8. Morphology of PMMA/PP/PS ternary blend (80/10/10): (a) without chemical etching; (b) after chemical attack with acetic acid; (c) after chemical attack with cyclohexane.

Analyzing the evolution of the morphology of systems composed by PMMA matrix, a subinclusion formation of PS in the core of PP is noticed, when the PP content is increased to 75 vol % (based on the dispersed phase). Luzinov et al.³⁹ studying the ternary systems composed by PS/SBR/PE (PS is the matrix phase) showed that a core-shell morphology is obtained with core of PE and shell of SBR, and subinclusions of SBR are found in the core of PE when the PE content is beyond the value for theoretical phase inversion, considering binary blends composed by PE/SBR. The following equation was used to predict the theoretical phase inversion, based on binary blends:

$$\frac{\eta_1}{\eta_2} = \frac{\Phi_1}{\Phi_2} \quad (5)$$

where η_1 and η_2 are the viscosities of the polymers at constant shear rate, corresponding to the processing velocity studied, and Φ_1 and Φ_2 are the volume fractions of polymers 1 and 2, respectively.

Using the above equation for binary blends of PP/PS, and considering the viscosity of the polymers at a shear rate of 115 s^{-1} , it was found that the volume fraction of PP to phase inversion is 34%. Thus, as observed by Luzinov et al.,³⁹ the presence of subinclusions of shell in the core of the droplets occurred to core contents much beyond the one for phase inversion, since the presence of shell subinclusions was observed only when the PP content increased to 75%.

To study the formation process of the PS subinclusions, blends with 60 vol % of PMMA and 40 vol % of dispersed phase were prepared. The obtained morphologies are presented in Figure 9. It can be seen that, as already observed in the 80/20 (matrix phase/dispersed phase) blends, the phenomenon of subinclusions of shell within the core occurred when the PP content is higher than 75 vol %, with the respect to the dispersed phase, corroborating the results of Luzinov et al.³⁹ who reported that subinclusions of the shell material in the core of the droplets represent the tendency of core to engulf the shell phase at core content larger than the theoretical phase inversion. The presence of a dispersed PS within PP (the core) could also be attributed to a high viscosity core (PP).⁶ During the initial stages of mixing, the shell could be immobilized by the core because of the high viscosity of the core, causing segregation effects in the core-shell structure. However, in the case of the blend studied here, the viscosity of PS shell is higher than the one of PP (the core). Therefore, a most likely explanation for the subinclusions observed here is that a phenomenon of phase inversion in the PS/PP binary system takes place when the PP content is much higher than the one for the theoretical phase inversion.

The results reported in this work indicate that, for the blends and viscosity ratios studied here, the core-shell morphology encountered is the one thermodynamically predicted by the spreading coefficient model, independently of the viscosity ratio of both dispersed phase, which is much above the one when PMMA is the matrix (1.95 at constant shear rate and 5.25 at constant shear stress), and much below the one when PP is the matrix (0.04 at constant shear rate and 0.22 at constant shear stress). This shows that a core-shell morphology is obtained even when the component with higher viscosity encapsulates the component with lower viscosity. Furthermore, these morphologies were obtained after only 2 min of mixing, even with PMMA as matrix, where the kinetic effect acts against the formation of core-shell droplets, and showed to be time-independent, since even after 10 min of mixing and 15 min of pressing, the obtained morphologies remained stable. The type of morphology did not change even when the composition ratio of the minor phases changed from 10/10 to 5/15. As a conclusion, differently from what was pointed out by some authors,^{12,13} it was observed that the viscosity ratio of the two minor phases did not influence the obtention of the core-shell morphology.

It can be also noticed, that the core-shell morphologies presented in parts a and b of Figure 6 differ with respect to the number of core particles inside the shell phase: in the case of the PMMA matrix, the droplets of PS contain only one particle of PP; in the case of the PP matrix, the droplets of the PS phase contain several particles of PMMA. The number of particles encapsulated inside the dispersed phase depends on an equilibrium between interfacial tension and viscosity ratio which both control the interfacial area. The lower the interfacial

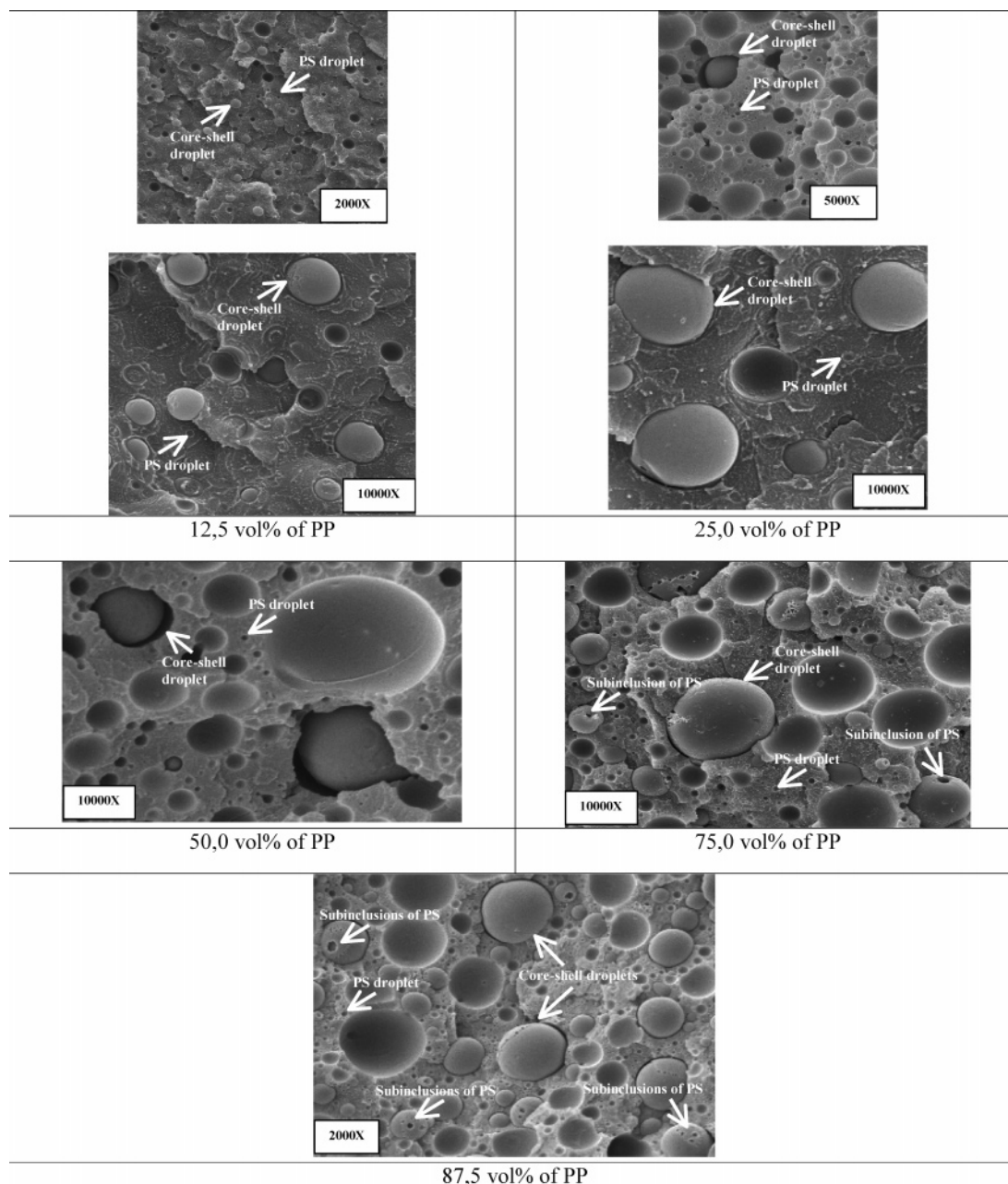


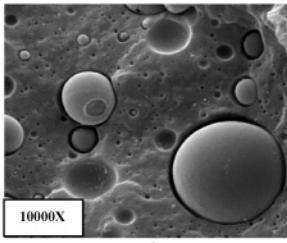
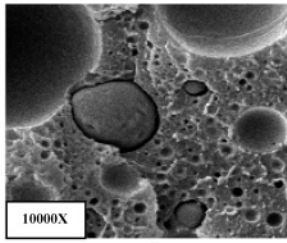
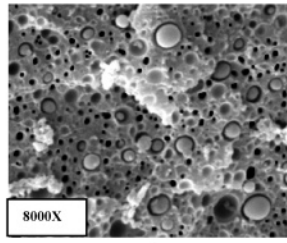
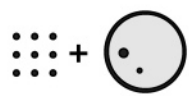
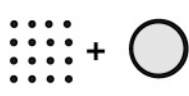
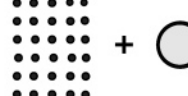
Figure 9. Morphology of PMMA/PP/PS blend: 60 vol % of PMMA and 40 vol % of PP + PS (PP content based on the dispersed phase).

tension, the easier it will be to form a large interfacial area. Also it is well-known that dispersed phase droplet size tends to decrease when the viscosity ratio dispersed phase/matrix decreases. It can be seen from Table 4 that the interfacial tension between PMMA and PS is more than three times lower than the interfacial tension between PP and PS. Also, the viscosity ratio PP/PS (in the case of a PMMA matrix) is much lower than the viscosity ratio PMMA/PS (in the case of a PP matrix). Both facts can explain the larger amount of PMMA particles.

Table 8 shows the results of the quantitative analysis of the morphologies of the blends for the three types of matrix. When PS and PP were the matrixes, the diameters of the dispersed phase of PMMA and PP (in the case of the matrix of PS) and of composite droplets (in the case of the matrix of PP) were evaluated directly from the micrographs. When PMMA was the matrix phase, to determine the volume average diameter (D_v) of the core-shell, and dispersed phase for each composition, the following procedure was adopted: first, the samples were cryogenically fractured and etched with cyclohexane, to remove

the PS. Microscopical observations of the samples, associated with quantitative analysis of the obtained morphology, showed that the core-shell droplets are present only in diameters above $0.3 \mu\text{m}$. The droplets having a diameter less than $0.3 \mu\text{m}$ were always hollow indicating that they must be formed of pure PS. The diameter of the PS dispersed phase was, therefore, determined directly using the micrographs considering all the drops with a diameter of less than $0.3 \mu\text{m}$. The external diameter (D_v of PS) of the composite droplets was obtained by direct measurement of all the droplets with $D_v > 0.3 \mu\text{m}$. The diameter of the core (D_v of PP) could then be obtained through the knowledge of the ratio between the surface area of PS (corresponding to the composite droplet area) and the surface area of PP (corresponding to the internal area of the droplet), which could be determined experimentally using the results of image analysis. These values are reported in Table 8. On the basis of the actual values of the diameter and the number of droplets determined using the micrographs, it was then possible to evaluate the actual composition of the blend, i.e., the fraction

Table 9. Microscopy of Samples Fractured of Blends of PMMA Matrix under Liquid Nitrogen and Etched with Cyclohexane^a

Composition		
80:15:05	80:10:10	80:05:15
		
		
% of core-shell = 18, 90 % of PS in core-shell = 2, 10 (shell) + 1, 5 (subinclusions) % of PP in core-shell = 15, 75 % of PS not included in core-shell = 2, 10 Experimental shell thickness = 0.09 μm .	% of core-shell = 16, 80 % of PS in core-shell = 6, 30 % of PP in core-shell = 10, 50 % of PS not included in core-shell = 4, 20 Experimental shell thickness = 0.12 μm	% of core-shell = 10, 50 % of PS in core-shell = 5, 25 % of PP in core-shell = 5, 25 % of PS not included in core-shell = 10, 50 Experimental shell thickness = 0.10 μm

^aSchematic representation of morphology was obtained of all blends (gray = PP and black = PS). The bold numbers presented in the table represent the PP and PS content based on blend composition, and the italic numbers represent the PP and PS content based on dispersed phase composition. All of these values were obtained experimentally as explained in the text.

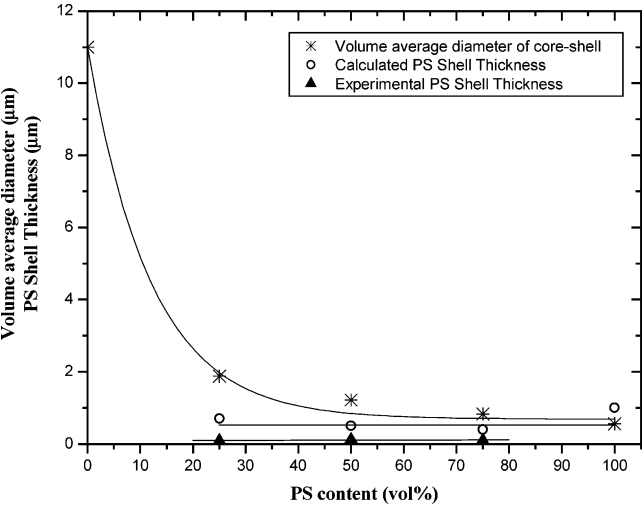


Figure 10. Volume average diameter, experimental PS shell thickness and calculated PS shell thickness as a function of PS content in the dispersed phase.

of composite droplets, of simple drops of PS, and of PS included in the composite droplets. Table 9 presents a summary of the morphological observations and the results obtained for the PMMA matrix.

For the PP matrix, only the results for the composition 5/15 are presented in Table 8, since for the composition 10/10 a cocontinuous phase morphology was obtained. When PS is the matrix phase, it can be observed from the results reported in Table 8 that the D_v of the PP droplets increases as the PP content in the blend increases, and the D_v of the PMMA droplets decreases as the PMMA content in the blend decreases.

It can be seen from the quantitative results reported in Tables 8 and 9 that the diameter of the composite droplets decreases when the concentration of PS increases. However, when PS

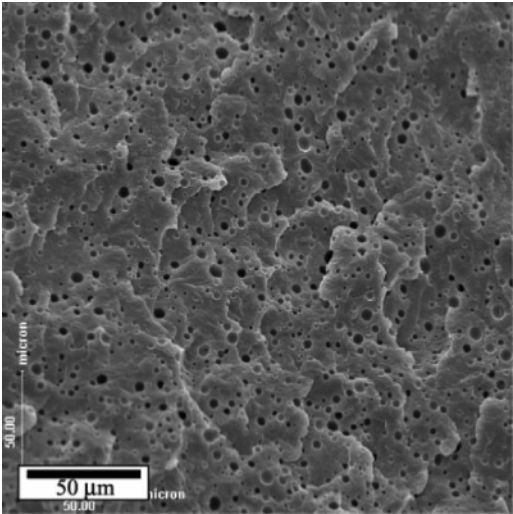


Figure 11. Morphology of PP/PS binary blend just before the addition of PMMA.

encapsulates PP, the higher viscosity of PS increases the core-shell droplet viscosities, which, in turn, increases the viscosity ratio between the dispersed phase and the matrix. This effect should cause an increase in the core-shell droplet size when the PS content increases, contrary to what is observed experimentally. The experimentally observed decrease of composite droplet diameter when the concentration of PS increases can only be therefore explained by the decrease of interfacial tension between the matrix and dispersed phase, caused by the encapsulation of PP by PS, which results in a reduction of droplet size. These results indicate that the thermodynamic forces (interfacial tension) compensate the effects of the viscosity ratio, decreasing the size of the droplets.

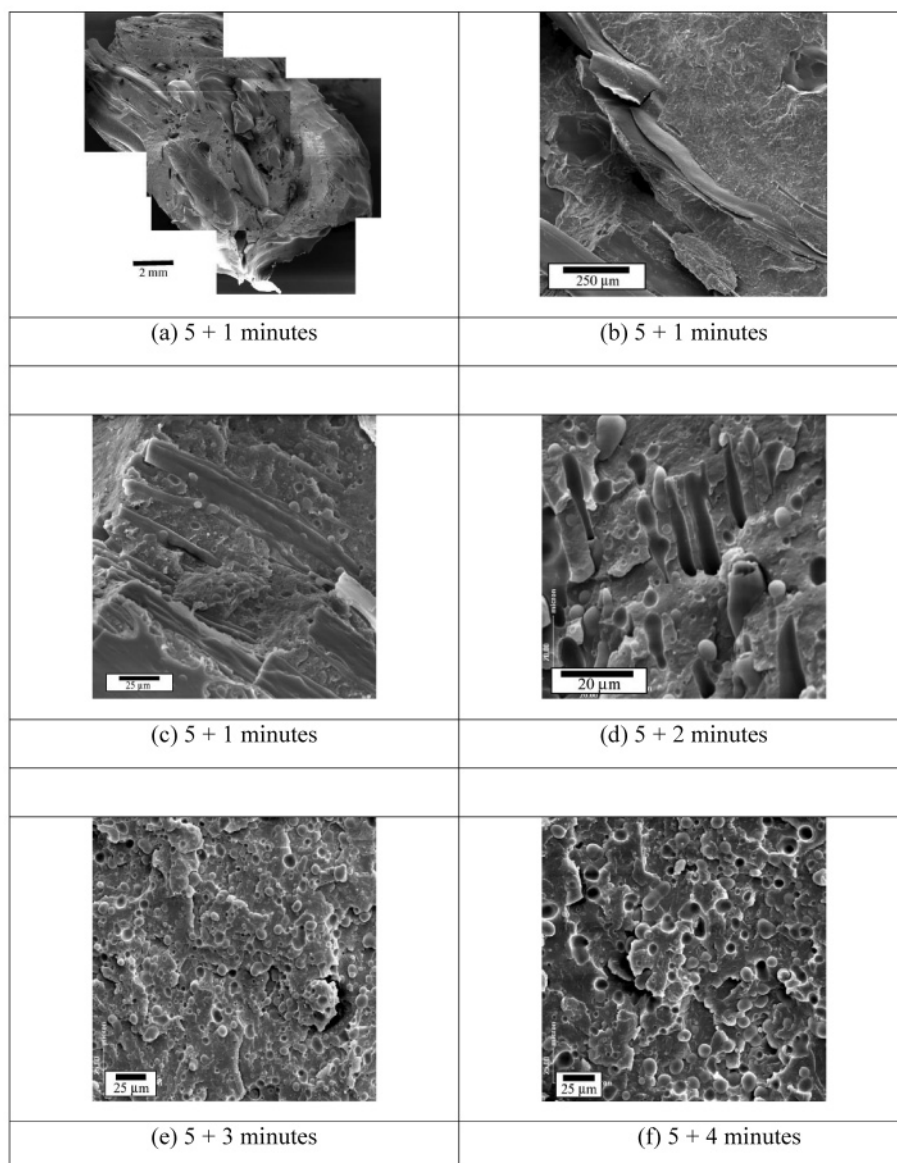


Figure 12. Evolution of the morphology of PMMA/PP/PS (10/80/10) blend as a function of time: (a) 5 + 1 min; (b) 5 + 1 min; (c) 5 + 1 min; (d) 5 + 2 min; (e) 5 + 3 min; (f) 5 + 4 min.

However, the thickness of the shell seems to remain constant within experimental error. Also, increasing the PS concentration results in an increase of the PS dispersed droplet content and an increase of the size of the simple PS dispersed phase. When the concentration of PS increases, the thickness of the shell remains constant, and more PS is dispersed as a third phase, inducing coalescence between the single drops of PS, which results in larger droplet diameters.

Figure 10 presents the values of D_v of the composite droplets and the experimental PS shell thickness as a function of PS content in the dispersed phase. The values of the PS shell thickness (H), calculated using the expression developed by Reignier and Favis^{4,6} (eq 6) are also reported in Figure 9:

$$H = \frac{1}{2} D_v [1 - \sqrt[3]{1 - \phi_{PS/DP}}] \quad (6)$$

where D_v is the volume average diameter of the core-shell droplets and $\phi_{PS/DP}$ is the volume fraction of PS based on the dispersed phase. In this work, as the fraction of PS in the core-shell droplets does not represent the fraction of PS present in

the blends, $\phi_{PS/DP}$ was determined using the actual PS content in the composite droplets (Table 9).

The results seem to indicate that PS acts as an emulsifier locating itself at the interface between PMMA and PP and reducing the diameter of PP dispersed phase. For contents of 25% of PS (relative to the dispersed phase), PP is completely encapsulated by the PS, resulting in a reduction in D_v from 11.00 (PMMA/PP binary blend) to 1.88 μm (80–15–05 ternary blend). Above 75% of PS (relative to the dispersed phase), the $D_v \times \text{PS}$ curve levels off reaching a value that corresponds to the one obtained for the PMMA/PS binary blend. Similar behavior was observed by Reignier and Favis,⁴ who studied the influence of concentration of PS on the morphology of high-density polyethylene (HDPE)/(PS + PMMA) (80/20) ternary blend, although the decrease of D_v (from 11 to 1.88 μm) is much larger than the one observed by Reignier and Favis.⁴ The larger difference observed in the present work can be explained by the difference of reduction of interfacial tension. When PMMA is the matrix and PS acts as an emulsifier (which is the case in this work), the interfacial tension decreases from 7.5 (PMMA/PP) to 1.7 (PMMA/PS) mN/m. When HDPE is the matrix and

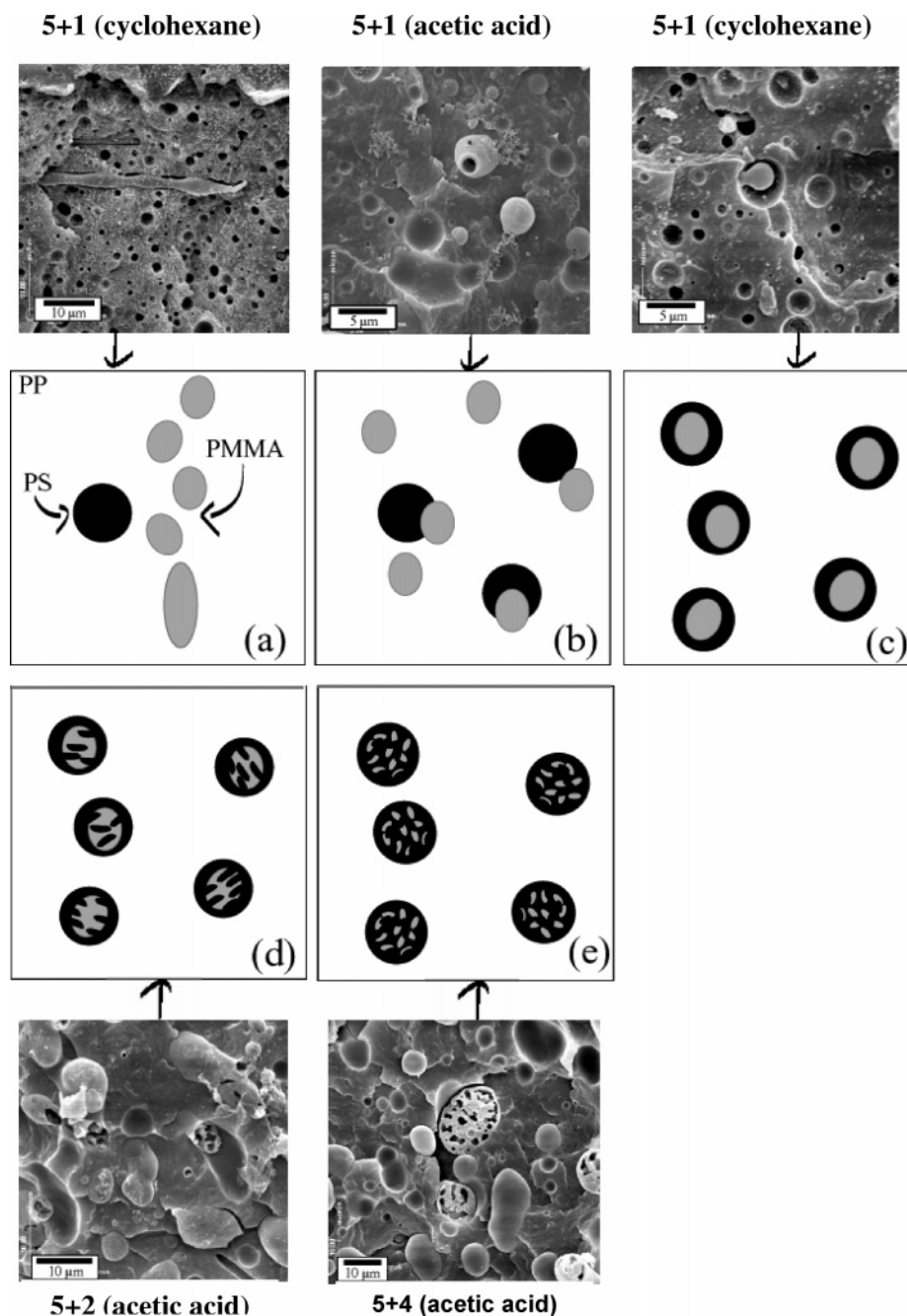


Figure 13. Evolution of the morphology of PMMA/PP/PS (10/80/10) blend as a function of time after solvent etching: (a) 5 + 1 min after etching using cyclohexane; (b) 5 + 1 min after etching using acetic acid; (c) 5 + 1 min after etching using cyclohexane; (d) 5 + 2 min after etching using acetic acid; (e) 5 + 4 min after etching using acetic acid.

PS acts as an emulsifier (case of Reignier and Favis^{4†} work) the interfacial tension decreases from 8.6 to 5.1 mN/m.

It can also be seen from Figure 10 that the value of the thickness of the shell of PS stays constant when the concentration of PS increases. The same behavior was observed for both the calculated and experimental values, although eq 5 seems to overestimate the value of the shell thickness. The trend observed for the shell thickness as a function of PS constant differs from the one observed by Reignier and Favis,⁴ who observed that the shell thickness of PS increased in the case of HDPE/PS/PMMA blend. In the system PMMA/PP/PS, after the complete encapsulation of the core (5% PS in the dispersed phase), the experimental PS shell thickness is not altered, but there is a reduction in the PS fraction present in the composite droplets, as a function of the increase of the PS content in the dispersed phase. The PS volume reduction contributes to the decrease of

the composite droplet size, since the viscosity ratio PS/PMMA is larger than the one for PP/PMMA. This factor, associated with the interfacial tension, can explain the reduction in D_v observed in blends with 5 to 15% of PS in the dispersed phase. Since the interfacial tension of PMMA/PS is much lower than the interfacial tension of PP/PS, the thermodynamical effect contributes more to the formation of pure PS droplets than it does to the encapsulation of PP by the PS. Moreover, analyzing the 60/40 systems presented in Figure 9, droplets of pure PS can already be observed in systems where the PS content is as low as 12.5%. Thus, low PS contents are already enough to encapsulate the PP, and the rest of PS goes to the matrix. In the system studied by Reignier and Favis,⁵ the shell/matrix interfacial tension (PS/PE) is much higher than the one of the shell/core (PS/PMMA), that is, in this case the thermodynamical factor favors the presence of PS at the interface PE/PMMA.

Therefore, corroborating the conclusions presented by the authors, the results presented in this paper show that the reduction in interfacial tension is the main driving force which controls the formation of core-shell structures in ternary blends.

3.4. Formation of Morphology. To study the formation of morphology of a ternary blend the morphology of several samples of a 10/80/10 HV-PMMA/PP/PS blend were observed. The samples were obtained according to the procedures summarized in Figure 2. Figure 11 shows the dispersed phase morphology of the PP/PS blend just before the addition of PMMA. The morphology of the binary blend consists of droplet dispersion of PS in PP. Figure 12 shows the evolution of the morphology of the ternary blend based on the results obtained in this study and the results obtained by Macosko et al.^{34,35} for binary blends. It can be seen from Figure 12 that the PMMA evolved from a pellet shape (Figure 12a) to a platelet-layer shape (Figure 12, parts b and c) and then toward long threads (Figure 12d) and dispersed drop shape (Figure 12, parts e and f) corroborating the results reported by Macosko et al.^{35,36} for binary blends. To understand the inclusion of PMMA into PS, other observations were done using selective dissolution. Figure 13 shows the evolution of the morphology of the ternary blend as a function of processing time using selective dissolution. It can be seen that during the first minute of processing the threads of PMMA break up into droplets with a size comparable to the ones of PS (Figure 13a) forming a double dispersion type morphology, then the PMMA penetrates the droplets of PS (Figure 13, parts b and c) forming a core-shell morphology with only one drop of PMMA inside a matrix. Subsequently, the core droplet of PMMA deforms and breaks up into smaller droplets (Figure 13, parts d and e).

4. Conclusion

In this work, the morphology of the PMMA/PP/PS ternary blend was studied. A mixture of separated PS droplets and core-shell morphologies (core of PP and shell of PMMA) was obtained when PMMA was the matrix, a core-shell morphology (with PS as shell and PMMA as core) was obtained when PP was the matrix, and separated dispersion was observed when PS was the matrix. The experimental observation corroborated the predictions of the minimal surface free energy theory only when PS was the matrix phase. The predictions of the spreading coefficient and dynamic interfacial tension models corroborate with most of the experimental results considering, in the case of dynamic interfacial tension model, the constant shear rate. However, when PMMA was the matrix phase, none of the studied models was able to predict the present of pure droplets of PS in the matrix.

It was shown that an increase of PS concentration for the blend with a matrix of PMMA resulted in a decrease of the composite droplet (with a core of PP and shell of PS) diameter but in a constant shell thickness. When the fraction of PS in the blend increased, a higher fraction of PS was dispersed as a third phase. These results indicate that PS acts as an emulsifier. In a binary blend of two polymers, **A** and **B**, a third polymer, **C**, can act as an emulsifier if the interfacial tension between **A** and **C** is lower than the one between **A** and **B** without being a compatibilizing agent. Moreover, when PMMA is the matrix phase, if the PP content is increased much beyond that for the theoretical phase inversion, the presence of shell subinclusions in the core can be observed.

The formation of morphology in the case of the PMMA/PP/PS blend was studied as a function of processing time. It was showed that when PMMA is added to the binary blend of PP/

PS, threads of PMMA are formed; they then break up into droplets with a size comparable to the ones of PS forming a double dispersion type morphology, and then the PMMA penetrates the drops of PS forming a core-shell morphology with only one drop of PMMA inside a matrix. Subsequently, the core droplet of PMMA deforms and breaks up into smaller droplets.

Acknowledgment. The authors would like to thank the FAPESP and the CAPES for financial support.

References and Notes

- Utracki, L. A. *Polym. Eng. Sci.* **1995**, *35*, 2–17.
- Guo, H. F.; Packirisamy, S.; Gvozdic, N. V.; Meier, D. J. *Polymer* **1997**, *38*, 785–94.
- Guo, H. F.; Gvozdic, N. V.; Meier, D. J. *Polymer* **1997**, *38*, 4915–23.
- Reignier, J.; Favis, B. D. *Macromolecules* **2000**, *33*, 6998–7008.
- Reignier, J.; Favis, B. D.; Heuzey, M. C. *Polymer* **2003**, *44*, 49–59.
- Reignier, J.; Favis, B. D. *Mater. Interfaces Electrochem. Phenom.* **2003**, *49*, 1014–23.
- Hobbs, S. Y.; Dekkers, M. E. J.; Watkins, V. H. *Polymer* **1998**, *29*, 1598–1602.
- Lee, M.; Tzoganakis, C.; Kim, J. M. *Proceedings of the Annual Technical Conference ANTEC*; Orlando, FL, 2000; SPE: Brookfield.
- Nauman, E. B.; He, D. Q. *Chem. Eng. Sci.* **2001**, *56*, 1999–2018.
- Urashita, S.; Kawakatsu, T.; Doi, M. *Prog. Theor. Phys. Suppl.* **2000**, *138*, 412–13.
- Horiuchi, S.; Matchariyakul, Y. K.; Kitano, T. *Macromolecules* **1997**, *30*, 3664–70.
- Nemirovski, N.; Siegmann, A.; Narkis, M. J. *Macromol. Sci.—Phys.* **1995**, *B34*, 459–75.
- Gupta, A. K.; Srinivasan, K. R. *J. Appl. Polym. Sci.* **1993**, *47*, 167–84.
- Lusinov, I.; Pagnoulle, C.; Jérôme, R. *Polymer* **2000**, *41*, 7099–109.
- Hemmati, M.; Nazokdast, H.; Panahi, H. S. *J. Appl. Polym. Sci.* **2001**, *82*, 1129–1137.
- Tchomakov, K. P.; Favis, B. D. *Proceedings of the Annual Technical Conference—ANTEC*; San Francisco, CA, 2002; SPE: Brookfield.
- Legros, A.; Carreau, P. J.; Favis, B. D.; Michel, A. *Polymer* **1997**, *38*, 5085–89.
- Kim, B. K.; Kim, M. S.; Kim, K. K. *J. Appl. Polym. Sci.* **1993**, *48*, 1271–78.
- Demarquette, N. R.; Kamal, M. R. *J. Appl. Polym. Sci.* **1998**, *70*, 75–87.
- Van Oene, H. J. *Colloid Interface Sci.* **1972**, *40*, 448–67.
- Bousmina, M.; Ait-Kadi, A.; Faisant, J. B. *J. Rheol.* **1999**, *43*, 415–33.
- Valera, T. S.; Demarquette, N. R.; Toffoli, S. M. *J. Polym. Eng.* **2004**, *24*, 409–433.
- Graebbling, D.; Muller, R.; Paliere, J. F. *Macromolecules* **1993**, *26*, 320–9.
- Gramespacher, H.; Meissner, J. J. *Rheol.* **1992**, *36*, 1127–41.
- Demarquette, N. R.; Souza, A. M. C.; Palmer, G.; Macaúbas, P. H. P. *Polym. Eng. Sci.* **2003**, *43*, 670–83.
- Demarquette, N. R. *Int. Mater. Rev.* **2003**, *48*, 247–69.
- Souza, A. M. C.; Demarquette, N. R. *Polymer* **2002**, *43*, 1313–21.
- Souza, A. M. C.; Demarquette, N. R. *Polymer* **2002**, *43*, 3959–67.
- Macaúbas, P. H. P.; Demarquette, N. R. *Polymer* **2001**, *42*, 2543–54.
- Morita, A. T.; Carastan, D. J.; Demarquette, N. R. *Colloid Polym. Sci.* **2002**, *280*, 857–64.
- Arashiro, E. Y.; Demarquette, N. R. *Mater. Res.* **1999**, *2*, 23–32.
- Carreau, P. J.; De Kee, D.; Chhabra, R. *Rheology of polymeric systems principles and applications*; Carl Hanser: Munich, Germany, 1997.
- Underwood, E. E. *Quantitative stereology*; Addison-Wesley: Mass, 1970.
- Laun, H. M. *J. Rheol.* **1986**, *30*, 459–501.
- Palmer, G.; Demarquette, N. R. *Polymer* **2003**, *44*, 3045–52.
- Wu, S. In *Polym. Interfacial and adhesion*; Marcel Dekker: New York, 1982.
- Wu, S. In *Polymer Handbook*, 4th ed.; Brandrup, J., Immergut, E. H., Grulke, E. A.; Eds.; John Wiley & Sons: New York, 1999.
- Xing, P. X.; Bousmina, M.; Rodrigue, D.; Kamal, M. R. *Macromolecules* **2000**, *33*, 8020–8034.
- Luzinov, I.; Xi, K.; Pagnoulle, C.; Huynh-Ba, G.; Jérôme, R. *Polymer* **1999**, *40*, 2111–2520.